Editors' Suggestion

Magnetoelastic properties in the high-temperature magnetic phase of the skyrmion compound $GdRu_2Si_2$

J. Sourd [1], D. A. Mayoh [2], G. Balakrishnan [2], M. Uhlarz [1], J. Wosnitza,[1,3] and S. Zherlitsyn [1]

[1] *Hochfeld-Magnetlabor Dresden (HLD-EMFL) and Würzburg-Dresden Cluster of Excellence ctd.qmat, Helmholtz-Zentrum Dresden-Rossendorf, 01328 Dresden, Germany*

[2] *Department of Physics, University of Warwick, Coventry CV4 7AL, United Kingdom*

[3] *Institut für Festkörper- und Materialphysik, TU Dresden, 01062 Dresden, Germany*

(Received 20 November 2025; revised 3 February 2026; accepted 9 March 2026; published 9 April 2026)

We investigated the magnetoelastic properties of a $GdRu_2Si_2$ single crystal under a magnetic field applied along the crystallographic [001] and [110] directions. We report a series of strong anomalies in the sound velocity that is consistent with the complex phase diagram reported previously for this compound. In particular, in our study we focus on the recently identified magnetic phase in the high-temperature region. We show that while this phase is easily destroyed for magnetic fields applied along [001], it is rather stable for fields along [110]. Furthermore, we introduce a Landau theory and a microscopic toy model describing the elastic response at zero field. We reproduce qualitatively the observed anomalies for different acoustic modes, which suggest that the high-temperature phase weakly breaks the symmetry between the [100] and [010] directions. We discuss candidate magnetic structures consistent with this high-temperature phase, based on the comparison of elastic anomalies for a few different magnetic states.

DOI: 10.1103/ht3d-1kj8

I. INTRODUCTION

The magnetism of metallic systems is very rich and complex due to the important role of itinerant electrons, which carry the spin density in a complex and self-interacting fashion [1]. In the rare-earth metals, however, the magnetic properties are often dominated by localized $4f$ electrons that host a large magnetic moment. From this perspective, one can separate two types of degrees of freedom: localized $4f$ magnetic moments that can behave quasiclassically on the one hand and conduction electrons that generate the magnetic interactions between the localized moments on the other hand [2]. This permits integrating out the contribution from the conduction electrons, and within second-order perturbation theory one obtains the Ruderman-Kittel-Kasuya-Yosida (RKKY) interaction between pairs of localized moments [3–5]. In this way, the RKKY scheme reduces the physics of interacting localized and itinerant electrons into a Heisenberg-like model of classical spins on a lattice, much easier to deal with.

RKKY interactions are long ranged and oscillatory, often driving incommensurate or spiral magnetic order with propagation vectors determined by the Fermi-surface topology. This framework successfully explains the evolution of magnetic structures across the rare-earth series [6]. More recently, RKKY systems have regained interest in the context of frustrated magnetic materials, with the appearance of topological spin textures such as magnetic skyrmions and vortices [7]. These textures can be stabilized either by Dzyaloshinskii-Moriya interactions and magnetic fields [8] or by higher-order anisotropic terms inherent to the RKKY mechanism itself [9,10]. Moreover, the itinerant nature of the electrons in RKKY systems provides unique opportunities to probe such textures via transport phenomena, including anomalous and topological Hall effects [11,12].

A paradigmatic example is $GdRu_2Si_2$, in which localized $4f$ moments of Gd ($S = 7/2$) couple through conduction electrons derived primarily from Ru $4d$ orbitals [13]. The multiband Fermi surface revealed by quantum-oscillation measurements [14] gives rise to competing exchange interactions and complex magnetic phases. Since Gd^{3+} ions carry negligible orbital moment, single-ion anisotropy is weak, implying that fourth-order RKKY processes play an essential role in stabilizing multi-Q states [15,16].

Although $GdRu_2Si_2$ has been studied for decades [17], it recently regained attention following the discovery of a skyrmion-lattice phase by resonant x-ray scattering [18]. Its magnetic phase diagram includes helical states characterized by propagation vectors $\mathbf{q}_1 = (0.22 \times 2\pi/a, 0, 0)$ and $\mathbf{q}_2 = (0, 0.22 \times 2\pi/a, 0)$, whose superposition forms a double-Q skyrmion lattice. Further studies have revealed additional topological stripelike and high-temperature magnetic phases [19,20], highlighting the remarkable richness of this system. In particular, the magnetic structure associated to the high-temperature phase remains unresolved [20].

In this work, we employ ultrasound techniques to explore the magnetoelastic coupling in $GdRu_2Si_2$. We focus on the recently reported high-temperature magnetic phase [20],

Published by the American Physical Society under the terms of the Creative Commons Attribution 4.0 International license. Further distribution of this work must maintain attribution to the author(s) and the published article's title, journal citation, and DOI.

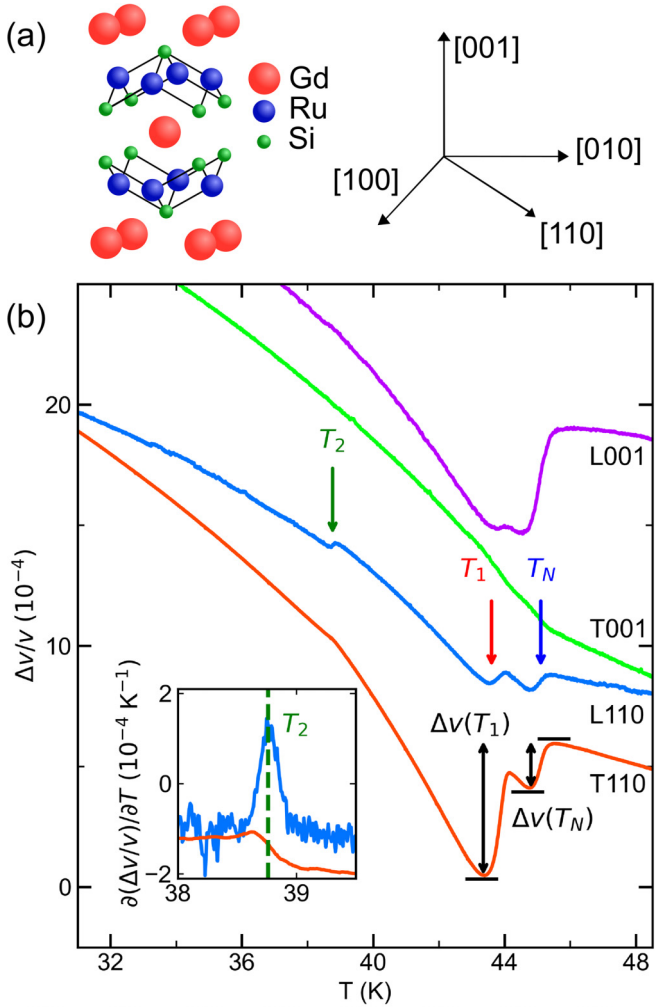


FIG. 1. (a) Crystal structure of $GdRu_2Si_2$. (b) Sound-velocity changes vs temperature at zero field for different elastic modes. The curves are arbitrarily shifted along the y axis for clarity. The inset shows the derivatives of the sound-velocity changes around T_2 for the modes L110 and T110.

examining its evolution under various magnetic-field orientations. Furthermore, we analyze the sound-velocity anomalies at zero field for different acoustic modes. With this method, we perform a detailed study of the coupling between the local $4f$ moments of Gd and the itinerant $4d$ electrons of Ru, and test different *ansätze* for the high-temperature phase. We show how the use of an ultrasound technique can be complementary to scattering probes such as neutrons or x-rays in order to investigate complex magnetic behavior in metallic magnets.

II. EXPERIMENT

We grew a single crystal of $GdRu_2Si_2$ [tetragonal $ThCr_2Si_2$-type structure, space group $I4/mmm$; see Fig. 1(a)] using the floating-zone method, as described in more detail in Ref. [19]. We selected a crystal of dimensions 2.5 mm×2.0 mm×1.5 mm, with the longest direction of 2.5 mm along the crystallographic [110] axis.

We applied magnetic fields and controlled the temperature in a Physical Property Measurement System, with sweep rates of 0.1 T/min and 0.5 K/min, respectively. We performed ultrasound experiments utilizing the transmission pulse-echo technique with phase-sensitive detection as described in Refs. [21,22]. We investigated four different elastic modes shown in Fig. 1(a), for which we introduce a compact notation. The first mode is a longitudinal wave with propagation **k** and polarization **u** along [001], and is denoted L001. The second longitudinal mode **k** ∥ **u** ∥ [110] is denoted L110. Furthermore, we studied two transverse modes, one with propagation **k** ∥ [110] and polarization **u** ∥ [001] denoted T001, and the second one with **k** ∥ [110] and **u** ∥ [1$\bar{1}$0] denoted T110. Thus, the two modes L001 and T001 are associated with atomic displacement along the c axis, while the two other modes L110 and T110 have both propagation and polarization in the (a, b) plane. We attached $LiNbO_3$ transducers (36°-Y cut and 41°-X cut for exciting longitudinal and transverse modes, respectively) to the polished surfaces of the single crystal. We used ultrasound frequencies between 60 and 90 MHz. This corresponds to a typical wavelength of 50 μm for the sound wave, much larger than the typical magnetic period of about 4 lattice spacing (≈2 nm).

TABLE I. Magnitude of the anomalies detected in the sound-velocity changes of $GdRu_2Si_2$ for the different elastic modes at zero field. The predicted anomalies of the different magnetic states $Helical_1$, $Helical_2$, $Double_q$, and $Double_q^*$ will be discussed in the theory section.

$10^{-4} \times \Delta v$	L001	T001	L110	T110
T_N	−4.4	0	−0.7	−2.0
T_1	−4.5	0	−1.2	−6.3
$Helical_1$	−5.2	0	−0.7	−0.4
$Helical_2$	−0.04	0	−0.01	0
$Double_q$	−5.2	0	−0.6	0
$Double_q^*$	−5.2	0	−0.7	−0.1

III. ZERO-FIELD RESULTS

We show our results at zero field in Fig. 1(b). We observe sharp anomalies on the $\Delta v/v$ curves at the Néel transition with $T_N = 45.1$ K. We detect the strongest anomaly for the mode L001, with a jump of $\Delta v/v = -4.4 \times 10^{-4}$. For T110 and L110 we also observe a jump, but smaller in magnitude. Finally, for T001, we detect only a kink at this temperature. Just below T_N, we observe further sharp anomalies at $T_1 = 43.8$ K with a notable jump of T110, a weaker jump in L110, and rather small anomalies for L001 and T001. The narrow window between T_1 and T_N corresponds to the high-temperature phase reported recently in [20]. We determine the sound velocity anomalies at $T_i = T_N$ or T_1 as $\Delta v(T_i) = [v(T_i) - v_i(45.5\ \mathrm{K})]/v_i(45.5\ \mathrm{K})$, as shown in Fig. 1(b). We summarize the results in Table I, which will be discussed later within the Landau theory.

At a lower temperature, we detect another anomaly at $T_2 = 38.8$ K, which corresponds to an additional phase boundary. It is associated with a small jump in L110 and a kink in T110 [and, respectively, as a peak and a step in the derivative of the sound velocities in the inset of Fig. 1(b)]. No clear anomaly is visible for L001 and T001 at this temperature. These results

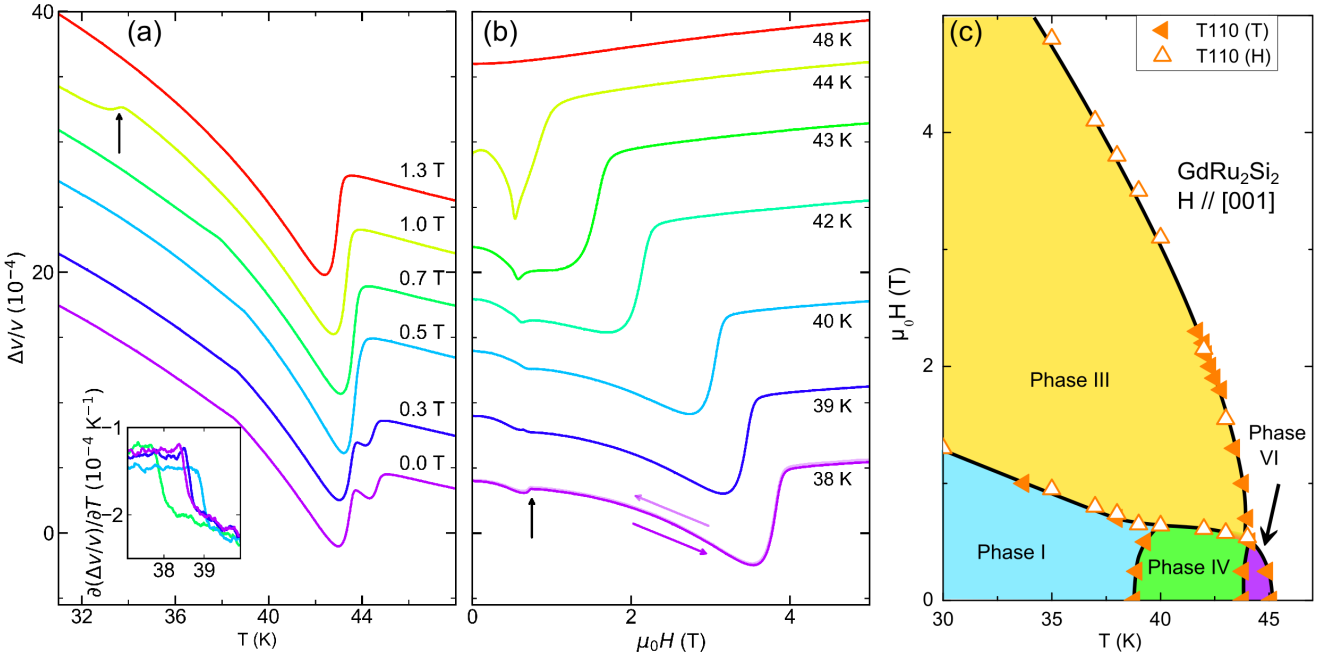


FIG. 2. Sound-velocity changes of the mode T110 vs temperature for selected magnetic fields (a), and vs field for selected temperatures (b). The curves are arbitrarily shifted along the y axis for clarity. (c) H-T phase diagram extracted from our ultrasound data, for magnetic fields applied along [001]. The black lines are guides to the eye.

are in accordance with previous thermal-expansion observations [23], where this transition does not show any anomaly along the c axis but a change of slope in the thermal expansion along the a axis.

From these zero-field results, we conclude that T110 is the most instructive: It is sensitive to all three transitions and shows anomalies of different magnitudes at T_N and T_1. This allows one to better distinguish the different phases. In the following, we will, thus, focus on this acoustic mode. We discuss the symmetry aspects related to the different acoustic modes in the theoretical section below.

IV. MAGNETIC FIELDS ALONG [001]

We show selected ultrasound data for magnetic fields applied along [001] in Fig. 2. From the anomalies observed in our ultrasound data, we construct the H-T phase diagram of Fig. 2(c), following the convention of Ref. [20] for phases I, III, IV, and VI.

In the temperature sweeps [Fig. 2(a)], we observe that phase VI is rapidly suppressed at a magnetic field of 0.5 T. At higher fields, the sound-velocity anomaly reflects a transition between the paramagnetic regime and phase III. We also note the evolution of the sound-velocity anomaly around T_2. This anomaly is a kink up to 0.7 T [also visible as a jump in the derivative, shown in the inset of Fig. 2(a)], and becomes a jump at 1 T, indicated by an arrow in Fig. 2(a). While the kink anomaly is associated with the transition from phase IV to phase I, the apparition of a jump might indicate the transition to a different phase, presumably from phase III to phase I.

We show selected field-sweep data in Fig. 2(b). We do not observe any significant hysteresis, as shown for the 38 K curve. We detect a sharp dip at 44 K, inside phase VI. This anomaly corresponds to the transition between phase VI and the paramagnetic phase. At lower temperatures the dip becomes much smaller, and we observe a second step-like anomaly at higher fields. This indicates a transition from phase IV to phase III, followed by a transition from phase III to the paramagnetic phase. Finally, at 38 K, the dip at low fields is replaced by a jump, indicated by an arrow in Fig. 2(b). This jump signals a transition from phase I to phase III at low fields.

V. MAGNETIC FIELDS ALONG [110]

We show selected ultrasound data and the extracted H-T phase diagram for magnetic fields applied along [110] in Fig. 3. In the temperature sweeps [Figs. 3(a)–3(c)], we observe a very rich set of anomalies. Remarkably, the anomaly associated to phase VI survives up to 9 T for this field direction. Furthermore, above 0.8 T, a kink anomaly appears inside phase VI, indicated by a black arrow in Fig. 3(a). This signals a potential intermediate phase that develops between phase VI and phase IV for this field direction, named phase VIb in our phase diagram. This kink is visible up to at least 6 T in Fig. 3(c).

At lower temperatures, the transition between phase IV and phase I is clearly visible as a kink in the sound velocity for the data at 0.5 T, indicated by a blue arrow in Fig. 3(a). For higher fields, this kink evolves into a jump, which suggests a transition between phase I and phase III, similar to our results observed for fields along [001]. Furthermore, we do not observe any evidence of transition between phase IV and phase III in the temperature sweeps up to 2.3 T. Only above 2.3 T, there appears a minimum (around 28 K), indicated by a red arrow in Figs. 3(b) and 3(c). This anomaly becomes more

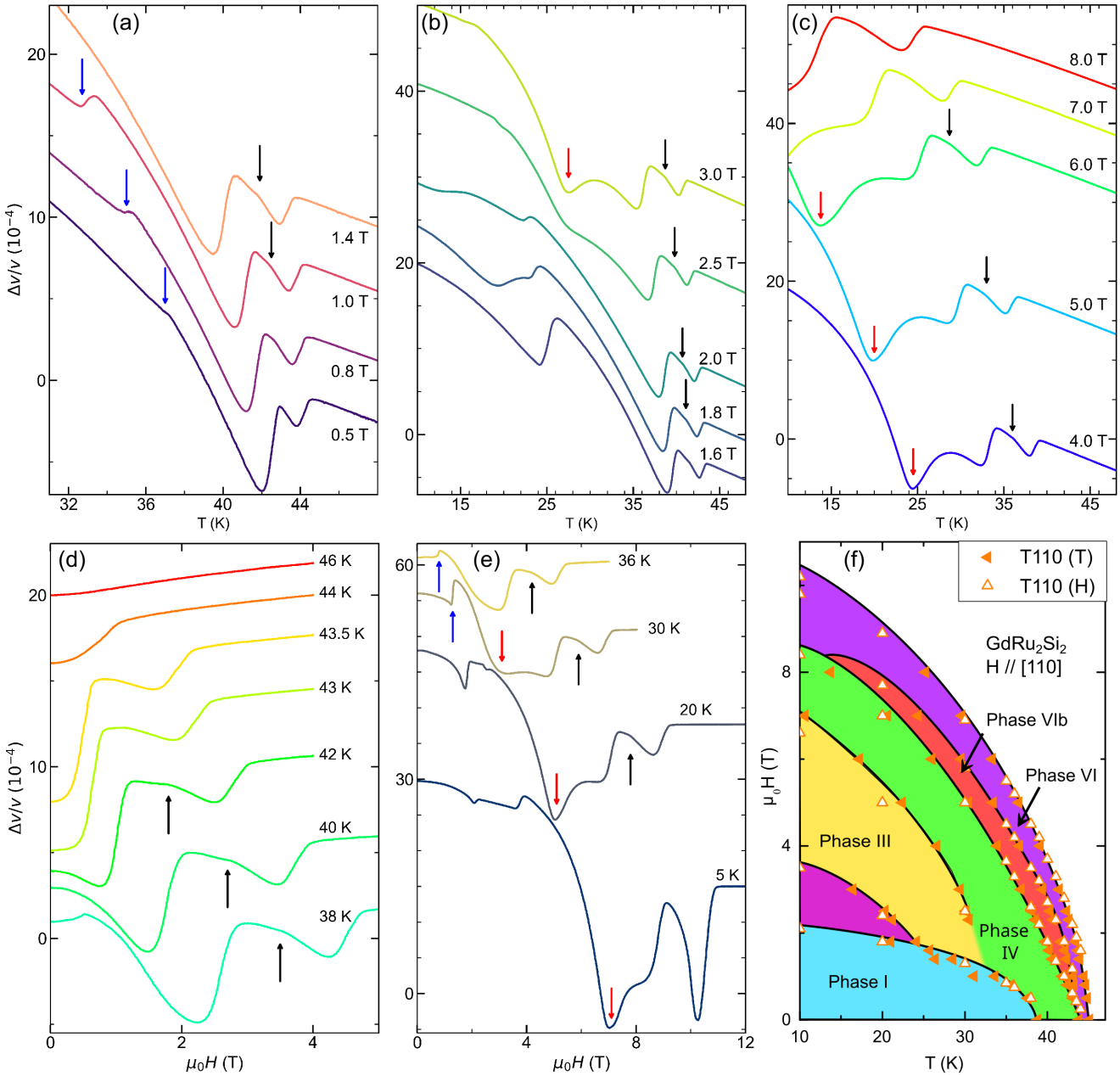


FIG. 3. Sound-velocity changes of the mode T110 vs temperature for selected magnetic fields (a)–(c), and vs field for selected temperatures (d) and (e). The curves are arbitrarily shifted along the *y* axis for clarity. (f) *H*-*T* phase diagram extracted from our ultrasound data, for magnetic fields applied along [110]. The black lines are guides to the eye.

pronounced with increasing fields and shifts progressively towards low temperatures. It corresponds to the transition between phase IV and phase III in our phase diagram [Fig. 3(f)]. This transition line could end in a critical point around 28 K and 2.2 T. Below 2.2 T, our results indicate presumably a crossover between phase IV and phase III.

We show selected field-sweep results in Figs. 3(d) and 3(e), which give us a consistent picture. At 44 K, we identify the transition into the paramagnetic regime with a jump in the sound velocity. At 43.5 K we observe two jumps, which correspond to transitions from phase IV to phase VI, followed by the transition from phase VI to the paramagnetic regime. Below 42 K, we detect the transition to phase VIb as a kink in the sound velocity, indicated by a black arrow in Fig. 3(d). We can follow this kink down to about 20 K [Fig. 3(e)]. It disappears at lower temperatures. At 38 K, we observe a kink at low fields, which indicates the transition between phase I and phase IV. At 36 K, this kink evolves into a jump [blue arrow in Fig. 3(e)], which indicates the transition from phase I to phase III. At 30 K and below, we detect the transition between phase III and phase IV, indicated by red arrows in Fig. 3(e). Finally, at 20 K and below, another intermediate phase appears between 2 and 4 T, in accordance with the earlier results of Ref. [15]. We summarize the *H*-*T* phase diagram in Fig. 3(f). Remarkably, this phase diagram shows that phase VI is very stable for this field direction.

VI. DISCUSSION

Our experimental data reveal a very rich phase diagram, which depends strongly on the magnetic field direction. Such directional sensitivity has been previously reported in Ref. [24] using magnetization, electrical transport, and magnetic resonant x-ray scattering. We confirm that when the magnetic field is rotated from the c axis to the (a, b) plane, the stability range of phase IV is enhanced, and additional phases appear. We also report additional phase boundaries, such as between phase III and phase IV for fields along [110], and between phase IV, phase V, and phase VI.

These differences arise from our choice of aligning the field along [110], as rationalized from analyzing the case of phase III. In Ref. [24], phase III is defined as a double-Q state with the magnetic moments perpendicular to both the propagation direction and the magnetic field. When the magnetic field is rotated from [001] to [100], the authors of Ref. [24] showed a continuous transformation of phase III, where the magnetic moments of the $\mathbf{q}_2 = (0, 0.22 \times 2\pi/a, 0)$ component rotate from $\mathbf{m}_2 \parallel [100]$ for $H \parallel [001]$ to $\mathbf{m}_2 \parallel [001]$ when H is along [100]. Since the condition that $\mathbf{m}_2$, $\mathbf{q}_2$, and $\mathbf{H}$ are perpendicular to each other cannot be satisfied for $H \parallel [110]$, we can expect new magnetic phases for this field direction.

Furthermore, we report very peculiar behavior for phase VI, which was not detected in [24]. This phase is suppressed at rather small fields applied along the [001] direction, while it remains pretty stable for fields along [110]. In this section, we propose a magnetic structure for this phase, based on our data for different acoustic modes. To this aim, we develop a phenomenological Landau theory and a microscopic model for the magnetoelastic couplings, which arise from the strain dependence of the RKKY interactions in $GdRu_2Si_2$.

A. Landau theory

Since phase VI has a phase boundary to the paramagnetic phase, the phenomenological Landau free energy is appropriate for its description. Following the neutron-diffraction results of Refs. [19,25], we assume that the local magnetization of the Gd atom at the site $\mathbf{r}_i$ can be written as

$$\mathbf{S}_i = S \sum_{\alpha} (\boldsymbol{\mu}_\alpha e^{i\mathbf{q}_\alpha \cdot \mathbf{r}_i} + \boldsymbol{\mu}_\alpha^* e^{-i\mathbf{q}_\alpha \cdot \mathbf{r}_i}), \tag{1}$$

where $\alpha = 1, 2$ allows for double-Q states and $\boldsymbol{\mu}_\alpha$ are normalized complex vectors such that $\sum_\alpha |\boldsymbol{\mu}_\alpha|^2 = 1$. Thus, with this formulation, the value of S defines the magnetic order parameter of a magnetic state characterized by the set $\{\boldsymbol{\mu}_\alpha, \mathbf{q}_\alpha\}$. From Refs. [19,25], we restrict the values of $\mathbf{q}_\alpha$ to $\mathbf{q}_1 = (0.22 \times 2\pi/a, 0, 0)$ and $\mathbf{q}_2 = (0, 0.22 \times 2\pi/a, 0)$. Defining the Fourier transform $\mathbf{S}_q = \frac{1}{N}\sum_i \mathbf{S}(\mathbf{r}_i) e^{-i\mathbf{q}\cdot\mathbf{r}_i}$, we assume that the magnetic contribution to the free energy at zero field can be written as in Refs. [26,27]:

$$\mathcal{F}_s = \frac{1}{2}\sum_q \alpha_q \mathbf{S}_q \cdot \mathbf{S}_{-q} + \frac{1}{4}\sum_{q_1,q_2,q_3} \beta_{q_1,q_2,q_3} (\mathbf{S}_{q_1} \cdot \mathbf{S}_{q_2})(\mathbf{S}_{q_3} \cdot \mathbf{S}_{-q_1-q_2-q_3}), \tag{2}$$

where α_q and β_{q_1,q_2,q_3} are phenomenological parameters. Inserting Eq. (1), we obtain the following magnetic free energy:

$$\begin{aligned}
\mathcal{F}_s &= \frac{A_q}{2} S^2 + \frac{B_q}{4} S^4, \\
A_q &= \sum_\alpha (\alpha_{q_\alpha} + \alpha_{-q_\alpha})(\boldsymbol{\mu}_\alpha \cdot \boldsymbol{\mu}_\alpha^*), \\
B_q &= 2\sum_{\alpha\alpha'} [2|\boldsymbol{\mu}_\alpha|^2 |\boldsymbol{\mu}_{\alpha'}|^2 \beta_{q_\alpha q_\alpha q_{\alpha'}} + |\boldsymbol{\mu}_\alpha \cdot \boldsymbol{\mu}_{\alpha'}|^2 \beta_{q_\alpha q_{\alpha'} q_{\alpha'}} \\
&\quad + \mathrm{Re}[(\boldsymbol{\mu}_\alpha \cdot \boldsymbol{\mu}_{\alpha'})^2] \beta_{q_\alpha q_{\alpha'} q_{\alpha'}}].
\end{aligned} \tag{3}$$

We then include the strains η_μ with the bare elastic constants $C^0_{\mu\nu}$ and the magnetoelastic couplings λ_μ, so that the total free energy can be written as

$$\mathcal{F} = \mathcal{F}_s + \frac{1}{2}\sum_\mu \lambda_\mu S^2 \eta_\mu + \frac{1}{2}\sum_{\mu\nu} C^0_{\mu\nu} \eta_\mu \eta_\nu. \tag{4}$$

In this form, our theory is similar to the Landau theory developed for the magnetoelastic coupling in $CsNiCl_3$ [28]. One should, in principle, include a term of the form $S^2\eta_\mu\eta_\nu$ quadratic in the order parameter and the strains. However, such coupling can only lead to a kink at the phase boundary, and we neglect such a contribution here. At the ordering temperature, the linear coupling between the strain η_μ and the square of the order parameter S^2 generates a jump of the elastic constants, which can be evaluated as

$$C_{\mu\nu} - C^0_{\mu\nu} = -\frac{\partial^2\mathcal{F}}{\partial S \partial \eta_\mu}\left(\frac{\partial^2\mathcal{F}}{\partial S^2}\right)^{-1}\frac{\partial^2\mathcal{F}}{\partial \eta_\nu \partial S} = -\lambda_\mu \lambda_\nu \chi_S, \tag{5}$$

where $\chi_S = S^2(\frac{\partial^2\mathcal{F}}{\partial S^2})^{-1}$. For $GdRu_2Si_2$, we expect that χ_S depends in a complicated way on the magnetic configuration through the terms A_q and B_q, wich contain high-order RKKY processes as described in Refs. [9,10]. However, χ_S is independent of the strain η_μ and we can take it as a phenomenological parameter. Thus, with this model the jumps $C_{\mu\nu} - C^0_{\mu\nu}$ depend on the strain symmetry (μ, ν) only through the magnetoelastic couplings $(\lambda_\mu, \lambda_\nu)$.

B. Magnetoelastic coupling λ_μ

In this section, we evaluate the different magnetoelastic couplings λ_μ from a microscopic toy model. We presume that the magnetic properties of $GdRu_2Si_2$ are due to the RKKY interactions, which originate from the nonlocal Kondo coupling between Gd $4f$ and Ru $4d$ orbitals. This assumption is justified by the fact that the major contribution of the density of states at the Fermi level is dominated by Ru $4d$ bands [13,29,30]. Denoting the Gd sites as i and i' and the Ru sites as j and j', we can write the RKKY Hamiltonian as

$$\begin{aligned}
\mathcal{H}_{\mathrm{RKKY}} &= -\sum_{ii'} J^{ii'}_{\mathrm{RKKY}} \mathbf{S}_i \cdot \mathbf{S}_{i'}, \\
J^{ii'}_{\mathrm{RKKY}} &= \sum_{jj'} J^{ij}_K J^{i'j'}_K \chi_c(\mathbf{r}_j - \mathbf{r}_{j'}),
\end{aligned} \tag{6}$$

where J^{ij}_K is the nonlocal Kondo coupling and $\chi_c(\mathbf{r})$ the spin susceptibility of the conduction electrons. In our case, we consider $J^{ij}_K = J_K$ if i and j are nearest neighbors as in Fig. 4, and zero otherwise. The nonlocal Kondo coupling has

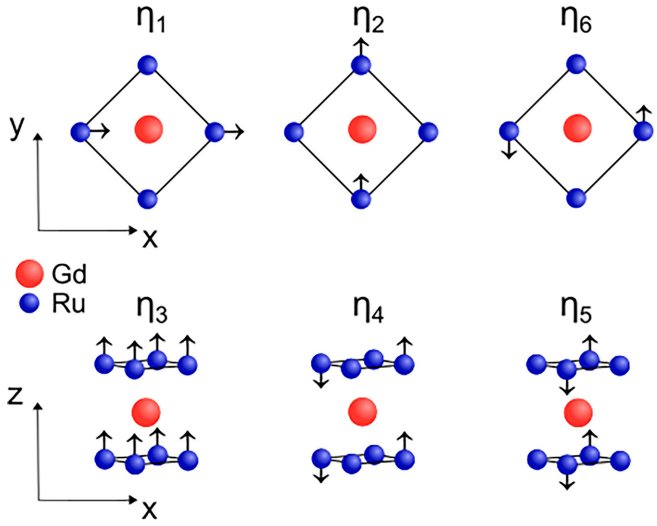


FIG. 4. Visualization of the different strains on nearest-neighbor Ru and Gd ions.

been introduced in the context of the paramagnetic heavy-fermion regime [31,32] and we propose here to extend it in the context of the magnetic RKKY regime. Specifically, in our case, it is an essential ingredient to obtain the interactions between Gd magnetic moments and the strains. We assume an isotropic anzatz for the Kondo interaction, which decreases exponentially with increasing the Gd-Ru bond distance $J_K^{ij} = J_{K0}^{ij}\exp(-|\mathbf{r}_{ij}|/\xi)$, with $\mathbf{r}_{ij} = \mathbf{r}_i - \mathbf{r}_j$. We introduce atomic displacements $\mathbf{u}_i$ by writing $\mathbf{r}_i = \mathbf{r}_i^0 + \mathbf{u}_i$, with $|\mathbf{u}_i|$ much smaller than a, the lattice spacing in the (a, b) plane. Then, we can expand the bond distance r_{ij} and the nonlocal Kondo coupling J_K^{ij} to first order in $|\mathbf{u}_i - \mathbf{u}_j|$, which gives

$$J_K^{ij} = J_{K0}^{ij} e^{-|\mathbf{r}_{ij}^0|/\xi}\left(1 - \sum_\mu \delta_\mu^{ij}\eta_\mu\right), \tag{7}$$

with the δ_μ^{ij} given by

$$\delta_1^{ij} = \frac{(r_{ij}^x)^2}{\xi r_{ij}}, \quad \delta_2^{ij} = \frac{(r_{ij}^y)^2}{\xi r_{ij}}, \quad \delta_3^{ij} = \frac{(r_{ij}^z)^2}{\xi r_{ij}},$$
$$\delta_4^{ij} = \frac{r_{ij}^x r_{ij}^z}{\xi r_{ij}}, \quad \delta_5^{ij} = \frac{r_{ij}^y r_{ij}^z}{\xi r_{ij}}, \quad \delta_6^{ij} = \frac{r_{ij}^x r_{ij}^y}{\xi r_{ij}}. \tag{8}$$

To get the magnetoelastic coupling, we insert this expression in the RKKY Hamiltonian (6) and keep only the terms linear in η_μ. We introduce the change of variables $i' = i + z$, $j = i + z_1$, $j' = i' + z_2$, and we obtain

$$\mathcal{H}_{\text{magn-el}} = \sum_{iz\mu} \lambda_\mu^z \eta_\mu \mathbf{S}_i \cdot \mathbf{S}_{i+z},$$
$$\lambda_\mu^z = \sum_{z_1 z_2} J_{K0}^{z_1} J_{K0}^{z_2} \left(\delta_\mu^{z_1} + \delta_\mu^{z_2}\right) \chi_c(z_1 - z - z_2). \tag{9}$$

Finally, using Eq. (1), we can write the final form for the magnetoelastic couplings as

$$\lambda_\mu = 4 \sum_{z\alpha} \lambda_\mu^z |\boldsymbol{\mu}_\alpha|^2 \cos(\mathbf{q}_\alpha \cdot \mathbf{z}). \tag{10}$$

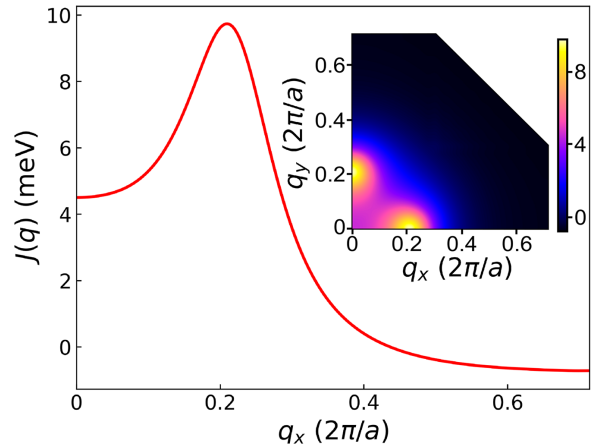


FIG. 5. Fourier transform $J(q)$ of the magnetic interactions up to 60 unit cells. The inset shows a colormap of $J(q)$ on the $q_z = 0$ plane of the Brillouin zone.

C. Application to $GdRu_2Si_2$

In order to evaluate λ_μ^z from Eq. (9), we take the simple ansatz of an Ornstein-Zernike form for the conduction-electron spin susceptibility [33,34], which reproduces the maxima coming from the nesting properties of the Fermi surface [29]:

$$\chi_c(z) = \frac{1}{N}\sum_q e^{iqz}\chi_q,$$
$$\chi_q = \chi_0 \sum_{q_\alpha = \pm q_1, \pm q_2} \frac{\zeta^{-2}}{\zeta^{-2} + (q - q_\alpha)^2}. \tag{11}$$

In this expression, the factor ζ can be seen as a coherence length, which controls the long-distance decay of the RKKY interactions. We choose $\zeta = 2a$, which generates a sufficiently fast decay that allows us to restrict the sum over z in Eq. (10) to the first 60 unit cells. Furthermore, we fix $J_K^2\chi_0 = 6$ μeV. With this choice, the Fourier transform of our magnetic coupling $J_{\text{RKKY}}^{ii'}$ shown in Fig. 5 reproduces qualitatively the results from *ab initio* calculations of Ref. [29]. This $J(q)$ is also in qualitative agreement with the recent inelastic neutron-scattering results of Ref. [35].

We considered the different magnetic states proposed for phase III and phase IV in Refs. [18,19,25,36]. From Eq. (9), we obtain the same contribution to the magnetoelastic energy from helical and amplitude-modulated phases. Thus, our method does not allow us to distinguish between them. Furthermore, from Eq. (9), we also notice that the direction of the magnetic moment is arbitrary. Thus, we can restrict ourselves to two different states: The single-Q helical state with wave vector $\mathbf{q}_1$ denoted Helical$_1$, and the double-Q state with wave vectors $\mathbf{q}_1$ and $\mathbf{q}_2$ denoted Double$_q$. The Helical$_1$ state has been proposed as a potential magnetic structure for phase IV [25]. We added a second helical state with wave vector $\mathbf{q}_1 + \mathbf{q}_2$ denoted Helical$_2$ for comparison, as well as an asymmetric double-Q state with unequal contributions of $\mathbf{q}_1$ and $\mathbf{q}_2$, denoted Double$_q^*$.

Upon evaluating the magnetoelastic couplings, we find that only the compression strains η_1, η_2, and η_3 contribute

TABLE II. Different magnetic phases defined by $\{\boldsymbol{\mu}_\alpha, \mathbf{q}_\alpha\}$, and the associated magnitude of the magnetoelastic couplings.

	Helical_1	Helical_2	Double_q	Double_q^*
$\boldsymbol{\mu}_1$	$\frac{1}{\sqrt{2}}(1,i,0)$	$\frac{1}{\sqrt{2}}(1,i,0)$	$\frac{1}{\sqrt{2}}(1,0,0)$	$\frac{1}{2}(1,0,0)$
$\mathbf{q}$	$\mathbf{q}_1$	$\mathbf{q}_1+\mathbf{q}_2$	$\mathbf{q}_1$	$\mathbf{q}_1$
$\boldsymbol{\mu}_2$			$\frac{1}{\sqrt{2}}(0,1,0)$	$\frac{\sqrt{3}}{2}(0,1,0)$
$\mathbf{q}'$			$\mathbf{q}_2$	$\mathbf{q}_2$
Λ_1 (meV Å)	0.7	0.1	0.7	0.7
Λ_2 (meV Å)	0.5	0.1	0.7	0.6
Λ_3 (meV Å)	1.7	0.2	1.7	1.7

significantly. This is a consequence of our assumption for the strain dependence of the Kondo interaction in Eq. (6), which contributes only to compression and stretching of the Gd–Ru bonds. Defining $\Lambda_\mu = \lambda_\mu \xi$, we summarize our results for the different states in Table II. The magnetoelastic couplings Λ_4, Λ_5, and Λ_6 are negligible. The relative values between the Λ_μ will be directly related to the size of the jumps in the sound velocity between each mode.

For all states, we found that the coupling Λ_3 dominates strongly. This becomes clear from Fig. 4, where the strain η_3 gives the largest number of Ru atoms contributing to the magnetoelastic coupling. The couplings Λ_1 and Λ_2 are equal in the Helical_2 and Double_q states, as expected by symmetry between the [100] and the [010] axes. In the Helical_1 and in the Double_q^* states, however, this symmetry is broken, and the degeneracy between Λ_1 and Λ_2 is lifted. Furthermore, we can distinguish the Helical_2 state by comparing the value of Λ_3, which is much smaller for the Helical_2 state, while it has the same value in the other three states.

From the relative values of the Λ_μ, we obtain directly the relative values of the jumps in the elastic constants thanks to Eq. (5). We evaluate the corresponding sound velocity jumps using $\rho v_{L001}^2 = C_{33}$, $\rho v_{T001}^2 = C_{44}$, $2\rho v_{L110}^2 = C_{11} + C_{12} + 2C_{66}$, and $2\rho v_{T110}^2 = C_{11} - C_{12}$. We obtain

$$\begin{aligned}
\Delta v_{L001} &= -K_{L001}\Lambda_3^2, \\
\Delta v_{T001} &= 0, \\
\Delta v_{L110} &= -K_{L110}\frac{\Lambda_1^2 + \Lambda_1\Lambda_2}{2}, \\
\Delta v_{T110} &= -K_{T110}\frac{\Lambda_1^2 - \Lambda_1\Lambda_2}{2},
\end{aligned} \tag{12}$$

where $K_i = \chi_S/2\rho\xi^2 v_i^2 = K/v_i^2$. From Eqs. (12), we conclude that no jump should be observed in the T001 mode, in accordance with our experimental data. We also see that $\Delta v_{T110} = 0$ if $\Lambda_1 = \Lambda_2$, i.e., when the [100] and [010] axes are equivalent, such as for the Helical_2 and Double_q states. In order to further compare our predictions with the experimental data, we fix the phenomenological parameter to $K = 3 \times 10^{10}$ $(\text{meV s})^{-2}$, and we use $v_{L001} = 4200$ m/s, $v_{T001} = 2800$ m/s, $v_{L110} = 4600$ m/s, and $v_{T110} = 2600$ m/s measured at $T = 50$ K. The resulting anomalies for the different magnetic states are given in Table I.

We propose that the transition into phase IV at $T = T_1$ can also be described within the Landau theory, since T_1 is very close to T_N. As shown in Table I, our prediction for the Helical_1 state matches well the anomalies observed at T_1, with a strong anomaly for the mode L001, no anomaly for T001, and a weak anomaly for L110. Only the anomaly for T110 is underestimated one order of magnitude. This discrepancy arises from the simplifying assumption of an isotropic Kondo interaction between the Gd and Ru ions in our minimal model, which strongly suppresses the coupling to bond-rotating transverse acoustic modes such as T110, compared to bond-stretching longitudinal acoustic modes. A more realistic treatment, including anisotropic coupling associated with the Ru $4d$ orbitals, would be required for a better quantitative agreement and lies beyond the scope of the present work. Nevertheless, our toy model is consistent with the assumption of a Helical_1 state for phase IV [25].

Finally, we compare our prediction for T_N, associated with the unknown phase VI. Both the Helical_1 and Double_q configurations give comparable jumps in L001, which matches our experimental data. At T_N, the anomaly in T110 is much weaker than at T_1 but yet is finite, which implies a partial symmetry breaking between [100] and [010]. Thus, phase VI might be an intermediate between the Helical_1 state at T_1, which maximally breaks this symmetry, and the Double_q state, which does not break this symmetry and thus gives no jump for T110. This leads us to propose that phase VI could correspond to an intermediate Double_q^* state, characterized by unequal amplitudes of the two propagation vectors $\mathbf{q}_1$ and $\mathbf{q}_2$. In our case we used $|\boldsymbol{\mu}_2|^2 = 3|\boldsymbol{\mu}_1|^2$ as shown in Table II.

An alternative source of symmetry breaking between [100] and [010] could be the small difference between $\mathbf{q}_1 = (0.220 \times 2\pi/a, 0, 0)$ and $\mathbf{q}_2 = (0, 0.225 \times 2\pi/a, 0)$ observed experimentally at low temperatures [19]. However, the magnitude of the sound velocity anomalies (10^{-4}) is significantly smaller than what is typically associated with a structural phase transition involving a phonon soft mode. This suggests that the observed effects are more naturally interpreted as magnetoelastic in origin rather than evidence for a structural instability.

VII. CONCLUSION

We investigated the low-temperature magnetoacoustic properties of single-crystalline $GdRu_2Si_2$ and identified a series of sharp anomalies in the sound velocity, enabling the construction of detailed magnetic phase diagrams for fields applied along the [001] and [110] directions.

We gave particular attention to the recently reported high-temperature phase VI. We find that this phase exhibits strong directional sensitivity: It is suppressed by modest fields of 0.5 T applied along [001], yet remains stable up to 9 T along [110]. Measurements of multiple acoustic modes at zero field further reveal distinctive magnetoelastic signatures associated with this phase.

To interpret these findings, we developed a Landau framework and a microscopic toy model describing the strain dependence of the RKKY interactions in $GdRu_2Si_2$. While our toy model is incapable of definitely discriminating between single-Q and multi-Q magnetic states, it allows us to capture qualitative trends and impose symmetry constraints on the different magnetic phases. In particular, we suggest

that the magnetic structure of phase IV strongly breaks the symmetry between the [100] and [010] direction, while this symmetry breaking is weaker but yet finite in phase VI. These findings are consistent with a helical order for phase IV, and with an asymmetric double-Q magnetic structure for phase VI.

Our results highlight the intimate coupling between lattice strain and itinerant-electron-mediated magnetism in $GdRu_2Si_2$, and demonstrate how ultrasound experiments can serve as a sensitive probe of multi-Q magnetic textures in metallic magnets.

ACKNOWLEDGMENTS

We acknowledge support from the Deutsche Forschungsgemeinschaft (DFG) through SFB 1143 (Project No. 247310070) and the Würzburg-Dresden Cluster of Excellence on Complexity, Topology and Dynamics in Quantum Matter – ctd.qmat (EXC 2147, Project No. 390858490), as well as the support of the HLD at HZDR, member of the European Magnetic Field Laboratory (EMFL). We further acknowledge support under the European Union's Horizon 2020 research and innovation program through the ISABEL project (No. 871106). The work at the University of Warwick was financially supported by two Engineering and Physical Sciences Research Council grants: Grant No. EP/T005963/1 and the U.K. Skyrmion Project Grant No. EP/N032128/1

DATA AVAILABILITY

The data that support the findings in this article are available from the authors upon reasonable request.

[1] M. Brando, D. Belitz, F. M. Grosche, and T. R. Kirkpatrick, Metallic quantum ferromagnets, Rev. Mod. Phys. **88**, 025006 (2016).

[2] A. Szilva, Y. Kvashnin, E. A Stepanov, L. Nordström, O. Eriksson, A. I Lichtenstein, and M. I. Katsnelson, Quantitative theory of magnetic interactions in solids, Rev. Mod. Phys. **95**, 035004 (2023).

[3] M. Ruderman and C. Kittel, Indirect exchange coupling of nuclear magnetic moments by conduction electrons, Phys. Rev. **96**, 99 (1954).

[4] T. Kasuya, A theory of metallic ferro-and antiferromagnetism on Zener's model, Prog. Theor. Phys. **16**, 45 (1956).

[5] K. Yosida, Magnetic properties of Cu-Mn alloys, Phys. Rev. **106**, 893 (1957).

[6] J. Jensen and A. Mackintosh, *Rare-Earth Magnetism: Structures and Excitations* (Oxford University Press, New York, 1991).

[7] S. Hayami and Y. Motome, Topological spin crystals by itinerant frustration, J. Phys.: Condens. Matter **33**, 443001 (2021).

[8] S. Muhlbauer, B. Binz, F. Jonietz, C. Pfleiderer, A. Rosch, A. Neubauer, R. Georgii, and P. Boni, Skyrmion lattice in a chiral magnet, Science **323**, 915 (2009).

[9] S. Hayami and Y. Motome, Multiple-Q instability by (d–2)-dimensional connections of Fermi surfaces, Phys. Rev. B **90**, 060402(R) (2014).

[10] S. Hayami, R. Ozawa, and Y. Motome, Effective bilinear-biquadratic model for noncoplanar ordering in itinerant magnets, Phys. Rev. B **95**, 224424 (2017).

[11] Y. Akagi and Y. Motome, Spin chirality ordering and anomalous Hall effect in the ferromagnetic Kondo lattice model on a triangular lattice, J. Phys. Soc. Jpn. **79**, 083711 (2010).

[12] T. Kurumaji, T. Nakajima, M. Hirschberger, A. Kikkawa, Y. Yamasaki, H. Sagayama, H. Nakao, Y. Taguchi, T. Arima, and Y. Tokura, Skyrmion lattice with a giant topological Hall effect in a frustrated triangular-lattice magnet, Science **365**, 914 (2019).

[13] T. Nomoto, T. Koretsune, and R. Arita, Formation mechanism of the helical Q structure in Gd-based skyrmion materials, Phys. Rev. Lett. **125**, 117204 (2020).

[14] N. Matsuyama, T. Nomura, S. Imajo, T. Nomoto, R. Arita, K. Sudo, M. Kimata, N. D. Khanh, R. Takagi, Y. Tokura, S. Seki, K. Kindo, and Y. Kohama, Quantum oscillations in the centrosymmetric skyrmion-hosting magnet $GdRu_2Si_2$, Phys. Rev. B **107**, 104421 (2023).

[15] A. Garnier, D. Gignoux, N. Iwata, D. Schmitt, T. Shigeoka, and F. Zhang, Anisotropic metamagnetism in $GdRu_2Si_2$, J. Magn. Magn. Mater. **140-144**, 899 (1995).

[16] A. Garnier, D. Gignoux, D. Schmitt, and T. Shigeoka, Giant magnetic anisotropy in tetragonal $GdRu_2Ge_2$ and $GdRu_2Si_2$, Phys. B (Amsterdam, Neth.) **222**, 80 (1996).

[17] M. Ślaski, A. Szytuła, J. Leciejewicz, and A. Zygmunt, Magnetic properties of $RERu_2Si_2$ (RE=Pr, Nd, Gd, Tb, Dy, Er) interm etallics, J. Magn. Magn. Mater. **46**, 114 (1984).

[18] N. Khanh, T. Nakajima, X. Yu, S. Gao, K. Shibata, M. Hirschberger, Y. Yamasaki, H. Sagayama, H. Nakao, L. Peng, *et al.*, Nanometric square skyrmion lattice in a centrosymmetric tetragonal magnet, Nat. Nanotechnol. **15**, 444 (2020).

[19] G. D. A. Wood, D. D. Khalyavin, D. A. Mayoh, J. Bouaziz, A. E. Hall, S. J. R. Holt, F. Orlandi, P. Manuel, S. Blügel, J. B. Staunton, O. A. Petrenko, M. R. Lees, and G. Balakrishnan, Double-Q ground state with topological charge stripes in the centrosymmetric skyrmion candidate $GdRu_2Si_2$, Phys. Rev. B **107**, L180402 (2023).

[20] L. Gries, T. Kleinbeck, D. A. Mayoh, G. D. A. Wood, G. Balakrishnan, and R. Klingeler, Uniaxial pressure effects, phase diagram, and tricritical point in the centrosymmetric skyrmion lattice magnet $GdRu_2Si_2$, Phys. Rev. B. **111**, 064419 (2025).

[21] B. Lüthi, *Physical Acoustics in the Solid State* (Springer, Berlin, Heidelberg, 2006), Vol. 148.

[22] A. Hauspurg, S. Zherlitsyn, T. Helm, V. Felea, J. Wosnitza, V. Tsurkan, K.-Y. Choi, S.-H. Do, M. Ye, W. Brenig, and N. B. Perkins, Fractionalized excitations probed by ultrasound, Phys. Rev. B **109**, 144415 (2024).

[23] J. Prokleška, J. Vejpravová, and V. Sechovský, Magnetostriction measurement of $GdRu_2Si_2$ single crystal, J. Phys.: Conf. Ser. **51**, 127 (2006).

[24] N. Khanh, T. Nakajima, S. Hayami, S. Gao, Y. Yamasaki, H. Sagayama, H. Nakao, R. Takagi, Y. Motome, Y. Tokura, *et al.*, Zoology of multiple-Q spin textures in a centrosymmetric tetragonal magnet with itinerant electrons, Adv. Sci. **9**, 2105452 (2022).

[25] J. Paddison, J. Bouaziz, A. May, Q. Zhang, S. Calder, D. Abernathy, J. Staunton, S. Blügel, and A. Christianson, Spin dynamics of the centrosymmetric skyrmion material $GdRu_2Si_2$, Cell Rep. Phys. Sci. **5**, 102280 (2024).

[26] J. N. Reimers, A. J. Berlinsky, and A.-C. Shi, Mean-field approach to magnetic ordering in highly frustrated pyrochlores, Phys. Rev. B **43**, 865 (1991).

[27] T. Okubo, S. Chung, and H. Kawamura, Multiple-q states and the skyrmion lattice of the triangular-lattice heisenberg antiferromagnet under magnetic fields, Phys. Rev. Lett. **108**, 017206 (2012).

[28] G. Quirion, X. Han, and M. L. Plumer, Magnetoelastic coupling within a landau model of phase transitions: Application to the frustrated triangular antiferromagnet $CsNiCl_3$, Phys. Rev. B **84**, 014408 (2011).

[29] J. Bouaziz, E. Mendive-Tapia, S. Blügel, and J. B. Staunton, Fermi-surface origin of skyrmion lattices in centrosymmetric rare-earth intermetallics, Phys. Rev. Lett. **128**, 157206 (2022).

[30] S. Eremeev, D. Glazkova, G. Poelchen, A. Kraiker, K. Ali, A. Tarasov, S. Schulz, K. Kliemt, E. Chulkov, V. Stolyarov, *et al.*, Insight into the electronic structure of the centrosymmetric skyrmion magnet $GdRu_2Si_2$, Nano. Adv. **5**, 6678 (2023).

[31] H. Weber and M. Vojta, Heavy-fermion metals with hybridization nodes: Unconventional Fermi liquids and competing phases, Phys. Rev. B **77**, 125118 (2008).

[32] J. Sourd, S. Tencé, E. Gaudin, and S. Burdin, Nonlocal Kondo coupling and selective doping from cerium f electrons in iron-based superconductors, Phys. Rev. B **109**, 045117 (2024).

[33] I. Eremin, P. Thalmeier, P. Fulde, R. K. Kremer, K. Ahn, and A. Simon, Large magnetoresistance and critical spin fluctuations in GdI_2, Phys. Rev. B **64**, 064425 (2001).

[34] A. Abanov, A. Chubukov, and J. Schmalian, Quantum-critical theory of the spin-fermion model and its application to cuprates: Normal state analysis, Adv. Phys. **52**, 119 (2003).

[35] G. Wood, J. Stewart, D. Mayoh, J. Paddison, J. Bouaziz, S. Tobin, O. Petrenko, M. Lees, P. Manuel, J. Staunton, *et al.*, A magnon band analysis of $GdRu_2Si_2$ in the field-polarized state, npj Quantum Mater. **10**, 39 (2025).

[36] Y. Yasui, C. Butler, N. Khanh, S. Hayami, T. Nomoto, T. Hanaguri, Y. Motome, R. Arita, T. Arima, Y. Tokura, *et al.*, Imaging the coupling between itinerant electrons and localised moments in the centrosymmetric skyrmion magnet $GdRu_2Si_2$, Nat. Commun. **11**, 5925 (2020).